A Short Introduction to Liquid Crystals

Mykola Tasinkevych

March 26, 2021

Contents

1 Classification

Here we discuss anisotropic fluids which, however, are uniform at least in one spatial dimension. Because these type of fluids combine the (partial) spatial uniformity of a simple liquid with the orientational anisotropy of a crystal, they are dubbed "Liquid Crystal". It is an intermediate state of matter which exhibits typical properties of a liquid such as fluidity, inability to support shear, formation and coalescence of droplets as well as some crystalline properties such as anisotropy in optical, electrical, and magnetic properties, or periodic arrangement of molecules in one or two spatial direction.

In general liquid crystals are composed of molecules (called "mesogens") with the "non-spherical" shape, for example rod- or disk-like one. A few typical mesogens are shown in Fig. (1). From a steric point of view, molecules are rigid rods with the breadth to width ratio from 3:1 to 20:1.

The anisotropic properties of liquid crystals are caused by the existence of a preferred orientation of mesogens with respect to each other. The axis which is parallel to this preferred orientation of the mesogens is called the director $\mathbf{n}$. Intuitively, $\mathbf{n}$ can be understood as the result of averaging over the different orientations of the molecular axes $\mathbf{w}$. Typically, orientations $\mathbf{w}$ and $-\mathbf{w}$ are equivalent which means that also $\mathbf{n}$ and $-\mathbf{n}$ are equivalent, i.e. the director is not a vector.

It is possible to classify different liquid crystalline phases (mesophases) based on, e.g., the dimension D of the spatially homogeneous directions, as is shown in Table 1:

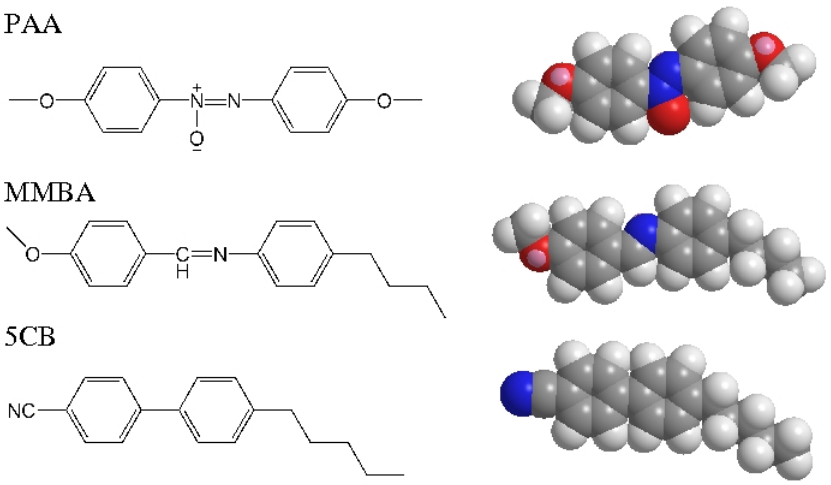

Figure 1: Typical mesogens forming liquid crystalline phases (mesophases). (PAA) *p*-azoxyanisole. From a rough steric point of view, this is a rigid rod of length $\sim$ 20Å and width $\sim$ 5Å. The nematic state is found at high temperatures (between 116^0C and 135^0C at atmospheric pressure). (MMBA) *N*-(*p*-methoxybenzylidene)-*p*-butylaniline. The nematic state is found at room temperatures (between 20^0C to 47^0C). Lacks chemical stability. (5CB) 4-pentyl-4'-cyanobiphenyl. The nematic state is found at room temperatures (between 24^0C and 35^0C).

Homogeneity	Isotropy	Mesophase
$D = 3$	$D = 3$	Isotropic, I
	$D < 3$	Nematic, N
$D = 2$	$D = 2$	Smectic-A, Sm_A
	$D < 2$	Smectic-C, Sm_C
$D = 1$		Columnar
$D = 0$	$D = 0$	Crystal

Liquid crystals which are obtained by melting a crystalline solid are called thermotropic. Additionally there are so-called lyotropic liquid crystals, where the phase transitions between mesophases are controlled by concentration rather then by temperature. Lyotropic liquid crystals most often are build from self-assembled surfactant molecules dissolved in water.

2 Anisotropic Susceptibility and Order Parameter Tensor

- One-particle angular distribution function -

We consider a system of N rod-like particles with positions $\mathbf{r}_i$ and orientation $\mathbf{w}_i$, $i = 1, .., N$. Next we

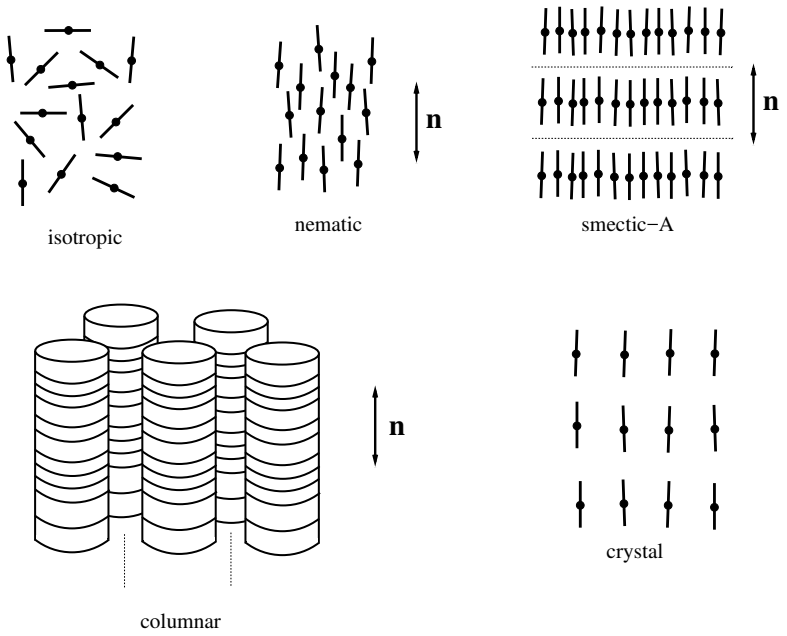

Figure 2: The arrangement of molecules in mesophases. In nematic phase the molecules tend to have the same alignment but their positions are not correlated. In smectic-A phase the molecules tend to lie in the planes with no configurational order within the planes and to be oriented perpendicular to the planes. Disc-shaped molecules self-assembled into columnar phase with the columns being ordered into $2D$ hexagonal lattice.

introduce one particle distribution function

$$\rho(\mathbf{r}, \mathbf{w}) = \langle \sum_{i}^{N} \delta(\mathbf{r} - \mathbf{r}_i)\delta(\mathbf{w} - \mathbf{w}_i) \rangle, \tag{1}$$

where $\langle ... \rangle$ denote thermal averaging over all possible $\mathbf{r}_i$ and $\mathbf{w}_i$. Integration over all orientations $\mathbf{w}$ gives rise to the orientation-independent one-particle distribution (number density)

$$\rho(\mathbf{r}) = \int_{S^2} \rho(\mathbf{r}, \mathbf{w}) d\Omega, \tag{2}$$

where $d\Omega$ is the solid angle element, and S^2 is the two-dimensional sphere. We also introduce one-particle angular distribution function

$$f(\mathbf{r}, \mathbf{w}) := \rho(\mathbf{r}, \mathbf{w})/\rho(\mathbf{r}). \tag{3}$$

We assume that the molecules have cylindrical symmetry and that $\eta_{||}$ and $\eta_{\perp}$ are the molecular magnetic susceptibilities along the molecular axis and the (degenerate) directions perpendicular to it. Then in an arbitrary coordinates

$$\eta_{ij} = \eta_{\perp}\delta_{ij} + \eta_a w_i w_j, \tag{4}$$

where the subscripts $i, j = 1, .., 3$, $\eta_a = \eta_{||} - \eta_{\perp}$ is the anisotropy of the molecular magnetic susceptibility, and δ_{ij} is the Kronecker delta. For usual nematic mesogens $\eta_{||} < 0$ and $\eta_{\perp} < 0$, i.e. the material are

diamagnetic.

- Magnetic susceptibility tensor -

A local magnetic field $\mathbf{H}$ at the position of a molecule induces in the molecule a dipole magnetic moment $\mathbf{m}$ with the components

$$m_i = \mu_0 \eta_{ij} H_j, \tag{5}$$

where μ_0 is the magnetic permeability of vacuum, and summation over the repeated indexes is implied. Because magnetic interactions between molecules are small, the local magnetic field is given mostly by the external magnetic field. This implies that the macroscopic magnetic susceptibility tensor $\boldsymbol{\chi}$ can be obtained from the sum of the molecular susceptibilities with appropriate averaging over the distribution function $\rho(\mathbf{r}, \mathbf{w})$. Consequently the local magnetization $\mathbf{M}(\mathbf{r})$ per unit volume in a liquid crystal in a uniform field may be calculated as

$$M_i(\mathbf{r}) = \mu_0 \int_{S^2} \rho(\mathbf{r}, \mathbf{w}) \eta_{ij} H_j d\Omega. \tag{6}$$

This leads to the following expression for the magnetic susceptibility

$$\begin{aligned} \chi_{ij}(\mathbf{r}) &= \mu_0 \int_{S^2} \rho(\mathbf{r}, \mathbf{w}) \eta_{ij} d\Omega \\ &= \mu_0 \rho(\mathbf{r}) \Big(\eta_\perp \delta_{ij} + \eta_a \int_{S^2} f(\mathbf{r}, \mathbf{w}) w_i w_j d\Omega \Big). \end{aligned} \tag{7}$$

Eq. (7) demonstrates that by measuring $\chi_{ij}(\mathbf{r})$ one also get an information about the angular distribution function $f(\mathbf{r}, \mathbf{w})$.

- Uniaxial nematic phase -

For uniaxial nematic phases, $f(\mathbf{r}, \mathbf{w})$ is rotationally symmetric with respect to $\mathbf{n}(\mathbf{r})$ and may be written as $f(\mathbf{r}, \mathbf{w}) = \bar{f}(\mathbf{r}, \cos\theta)$; θ is the angle between the director $\mathbf{n}(\mathbf{r})$ and the molecular axis $\mathbf{w}$. We introduce a local spherical coordinates with the polar axis parallel to $\mathbf{n}(\mathbf{r})$. Then the molecular axis

$$\mathbf{w} = \begin{pmatrix} \sin\theta\cos\phi \\ \sin\theta\sin\phi \\ \cos\theta \end{pmatrix},$$

and

$$\int_{S^2} f(\mathbf{r}, \mathbf{w}) w_i w_j d\Omega = \int_0^\pi \sin\theta \bar{f}(\mathbf{r}, \cos\theta) d\theta \int_0^{2\pi} w_i w_j d\phi. \tag{8}$$

Because

$$\mathbf{w}\mathbf{w}^T = \begin{pmatrix} \sin^2\theta\cos^2\phi & \sin^2\theta\cos\phi\sin\phi & \sin\theta\cos\theta\cos\phi \\ \sin^2\theta\cos\phi\sin\phi & \sin^2\theta\sin^2\phi & \sin\theta\cos\theta\sin\phi \\ \sin\theta\cos\theta\cos\phi & \sin\theta\cos\theta\sin\phi & \cos^2\theta \end{pmatrix}, \tag{9}$$

we obtain

$$\int_0^{2\pi} \mathbf{w}\mathbf{w}^T d\phi = \pi \begin{pmatrix} 1-\cos^2\theta & 0 & 0 \\ 0 & 1-\cos^2\theta & 0 \\ 0 & 0 & 2\cos^2\theta \end{pmatrix}. \tag{10}$$

Now the expression for the magnetic susceptibility tensor in Eq. (7) takes the form

$$\boldsymbol{\chi}(\mathbf{r}) = \mu_0\rho(\mathbf{r}) \begin{pmatrix} \eta_\perp + \frac{\eta_a}{2}(1-\langle\cos^2\theta\rangle_\theta & 0 & 0 \\ 0 & \eta_\perp + \frac{\eta_a}{2}(1-\langle\cos^2\theta\rangle_\theta & 0 \\ 0 & 0 & \eta_\perp + \eta_a\langle\cos^2\theta\rangle_\theta \end{pmatrix}. \tag{11}$$

In Eq. (11) $\langle ... \rangle_\theta := \int_{S^2} f(\mathbf{r},\mathbf{w})...d\Omega = 2\pi\int_0^\pi \sin\theta \bar{f}(\mathbf{r},\cos\theta)...d\theta$. From Eq. (11) we obtain for the anisotropy $\chi_a(\mathbf{r}) = \chi_{||}(\mathbf{r}) - \chi_\perp(\mathbf{r})$ of the macroscopic magnetic susceptibility tensor

$$\chi_a(\mathbf{r}) = \mu_0\rho(\mathbf{r})\eta_a\frac{1}{2}\left(3\langle\cos^2\theta\rangle_\theta - 1\right) = \mu_0\rho(\mathbf{r})\eta_a S(\mathbf{r}) \tag{12}$$

where we have introduced a scalar orientational order parameter

$$S(\mathbf{r}) = \frac{1}{2}\left(3\langle\cos^2\theta\rangle_\theta - 1\right); \tag{13}$$

and where $\chi_{||}$ and $\chi_\perp$ are the magnetic susceptibilities along the local nematic director $\mathbf{n}(\mathbf{r})$ (assumed here to be along $z-$axis) and the two (degenerate) directions perpendicular to it. It is easy to check that in the isotropic phase when $\bar{f} = \frac{1}{4\pi}$, $S = 0$ and as the result also $\chi_a = 0$, as supposed to be for an isotropic material. $\chi_\perp$ may be expressed via S as $\chi_\perp(\mathbf{r}) = \mu_0\rho(\mathbf{r})\left(\frac{\eta_{||}+2\eta_\perp}{3} - \frac{\eta_a}{3}S(\mathbf{r})\right)$. In arbitrary coordinate system

$$\chi_{ij}(\mathbf{r}) = \chi_\perp(\mathbf{r})\delta_{ij} + \chi_a n_i(\mathbf{r})n_j(\mathbf{r}). \tag{14}$$

- Order parameter tensor

In order to describe the nematic orientational ordering we introduce a tensorial order parameter $\mathbf{Q}$ defined as the deviatoric part of the susceptibility tensor $\boldsymbol{\chi}$

$$\mathbf{Q} := \boldsymbol{\chi} - \frac{1}{d} Tr \boldsymbol{\chi}. \tag{15}$$

$\mathbf{Q}$ is a symmetric traceless tensor. In general it has three different eigenvalues, which corresponds to so-called biaxial nematic. For uniaxial susceptibility as in Eq. (14), the order tensor may be presented in the form

$$\mathbf{Q} = \chi_a \left(n_i n_j - \frac{1}{3} \delta_{ij} \right). \tag{16}$$

Eq. (16) shows, that the nematic director $\mathbf{n}$ is the eigenvector of $\mathbf{Q}$ which correspond to the maximal eigenvalue

$$Q_{max} = \frac{2}{3} \chi_a = \frac{2}{3} \mu_0 \eta_a \rho S. \tag{17}$$

3 Isotropic-Nematic Phase Transition in Onsager Model

In this part we discuss a "simple" model introduced by Onsager in [1] in order to discuss the nematic-to-isotropic phase transition. Consider an ensemble of long cylindrical particles with the diameter D and the length L interacting pairwise via the hard-core potential $\mathcal{V}(\mathbf{1}, \mathbf{2})$ which depends on both positions and orientations of the molecules: $\mathbf{1} = (\mathbf{r}_1, \mathbf{w}_1)$. Onsager has shown how the Mayer cluster theory may be used to give an expansion for the equation of state of this system [1]. Onsager's expression for the Helmholtz free energy is written in terms of the single-particle distribution function, $\rho(\mathbf{1}) \equiv \rho(\mathbf{r}_1) f(\mathbf{r}_1, \mathbf{w}_1)$

$$\beta F[\rho] = \int \rho(\mathbf{1}) \Big(\ln(\rho(\mathbf{1}) \Lambda^3) - 1 - \beta\mu + \beta U(\mathbf{1}) \Big) d(\mathbf{1}) - \frac{1}{2} \int f^*(\mathbf{1}, \mathbf{2}) \rho(\mathbf{1}) \rho(\mathbf{2}) d(\mathbf{1}) d(\mathbf{2}). \tag{18}$$

Here $d(\mathbf{i}) = d^3 r_i d\Omega_i$, $\beta = 1/k_\mathrm{B} T$, $\Lambda = \sqrt{2\pi\hbar^2\beta/m}$ is the thermal de Broglie wavelength, μ is the chemical potential, $U(\mathbf{1})$ is the external potential energy. The Mayer f-function

$$f^*(\mathbf{1}, \mathbf{2}) = \mathrm{e}^{-\beta \mathcal{V}(\mathbf{1}, \mathbf{2})} - 1 = \begin{cases} -1, & \text{particles intersect} \\ 0, & \text{otherwise.} \end{cases} \tag{19}$$

Below we assume that $U(\mathbf{1}) = 0$, and $\rho(\mathbf{r}) = \bar{\rho} = const$. Then

$$\beta F[\rho] = V\bar{\rho}\Big(\int_{S^2} f(\mathbf{w})\left(\ln(\bar{\rho}\Lambda^3) - 1 - \beta\mu + \ln f(\mathbf{w})\right) d\Omega + \tag{20}$$

$$\frac{\bar{\rho}}{2}\int_{S^2}\int_{S^2} E(\mathbf{w}_1, \mathbf{w}_2))f(\mathbf{w}_1)f(\mathbf{w}_2)d\Omega_1 d\Omega_2\Big). \tag{21}$$

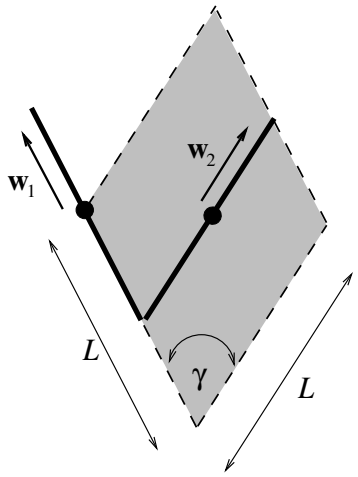

Figure 3: The excluded volume E of two hard rods depends on the angle γ between their axes $\mathbf{w}_1$ and $\mathbf{w}_2$. E is minimum for the parallel alignment, $\gamma = 0$, and maximum for perpendicular alignment $\gamma = \pi/2$. For $D \ll L$ we can neglect the ends effects leading to $E(\mathbf{w}_1, \mathbf{w}_2)) \approx 2DL^2|\sin\gamma|$.

with the excluded volume (see Fig. 3)

$$E(\mathbf{w}_1, \mathbf{w}_2) = -\int_V f^*(\mathbf{r}, \mathbf{w}_1, \mathbf{w}_2)d^3r \approx 2DL^2|\sin\gamma| \tag{22}$$

of one particle oriented at $\mathbf{w}_1$ with another particle oriented at $\mathbf{w}_2$. Because $\int_{S^2} f(\mathbf{w})d\Omega = 1$, the $f(\mathbf{w})-$dependent part of the functional in Eq. (21) has the form

$$\mathcal{F}[f] = \int_{S^2} f(\mathbf{w})\ln f(\mathbf{w})d\Omega + \bar{\rho}DL^2\int_{S^2}\int_{S^2}\sqrt{1-\mathbf{w}_1\mathbf{w}_2}f(\mathbf{w}_1)f(\mathbf{w}_2)d\Omega_1 d\Omega_2. \tag{23}$$

Now the objective is to minimize the functional (23) with respect to the angular distribution function $f(\mathbf{w})$. The normalization condition for $f(\mathbf{w})$ can be directly introduced in Eq. (23) by adding the term

$$\lambda\left(\int_{S^2} f(\mathbf{w})d\Omega - 1\right), \tag{24}$$

where λ is a Lagrange multiplier. The equilibrium $f(\mathbf{w})$ that minimizes the free energy functional (23) is a solution of the following Euler–Lagrange equation

$$\ln f(\mathbf{w}) = \lambda - 1 - 2\bar{\rho}DL^2 \int_{S^2} \sqrt{1 - \mathbf{w}\mathbf{w}_1} f(\mathbf{w}_1) d\Omega_1. \tag{25}$$

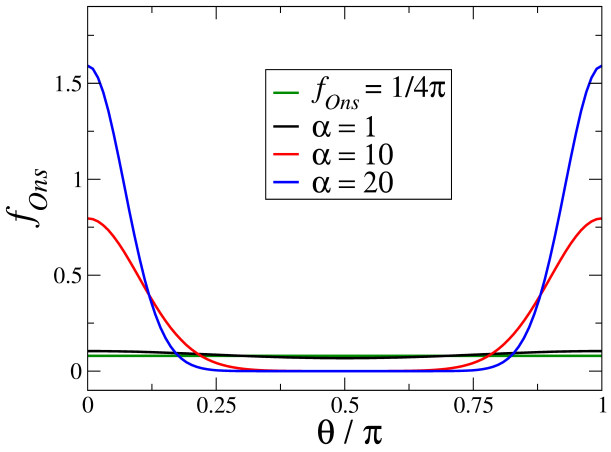

Figure 4: Onsager's trial function Eq. (26) with α as an variational parameter. For $\alpha \to 0$, $f_{Ons} \to 1/(4\pi)$, i.e. isotropic distribution of molecular axes. For $\alpha \neq 0$, f_{Ons} exhibits two picks at $\theta = 0, \pi$, which become sharper as α grows.

Equation (25) always has an "isotropic" solution $f(\mathbf{w}) = 1/(4\pi)$. However for large enough values of the dimensional parameter $\bar{\rho}DL^2$ Eq. (25) also admits anisotropic solution describing the nematic phase. The exact solution is not known, and approximate one can be obtained numerically. Onsager employed a one-parameter variational *Ansatz*

$$f_{Ons}(\mathbf{w}; \alpha) = \frac{\alpha}{4\pi \sinh \alpha} \cosh(\alpha \cos\theta). \tag{26}$$

The prefactor is chosen to fulfill the normalization condition, and α is the variational parameter. We recall that θ is the angle between the molecular axis and the nematic director. Substituting Eq. (26) into the expression for the free energy functional in Eq. (23) and minimizing the resulting function with respect to α one may calculate the phase boundary between the nematic and isotropic phases. In this case the parameter controlling the phase behavior is the rods' volume fraction $\phi = \bar{\rho}\pi D^2 L/4$.

In the isotropic phase $\alpha = 0$, and α is large in the nematic phase $\alpha_{nem} \simeq 19$. Larger values of α make the *Ansatz* function more peaked at $\theta = 0, \pi$ as is shown in Fig. 4. Onsager found that at the coexistence the volume fractions of the nematic and isotropic phases $\phi_{nem} = 4.5D/L$ and $\phi_{iso} = 3.3D/L$, respectively. This values demonstrate that the transition occurs for rather large aspect rations L/D. The free energy functional in Eq. (18) is based on the second-order virial expansion, therefore Onsager's results are applicable only for small volume fractions $\phi \ll 1$.

The physical mechanism responsible for the emergence of the nematic phase is related to the competition between translational and orientational entropies. Thus, the ideal-gas part in the Onsager functional, the first integral in the rhs. of Eq. (23), is independent on the density $\bar{\rho}$ and prefers the isotropic orientation of the rods. Contrary, the excluded volume part of Eq. (23) grows with $\bar{\rho}$ and prefers orientational configurations with as small volume per particle as possible, i.e. nematic phase. At sufficiently large densities, the entropy loss caused by the restriction of the orientational degrees of freedom can be compensated by the entropy gain due to the decrease of the excluded volume. In other words, in the isotropic phase the orientational entropy dominates, while in the nematic phase – the translational one.

4 Landau-de Gennes Theory

- Phenomenological free energy functional -

In the following we will consider purely phenomenological approach to the orientational ordering which is based solely on the tensor order parameter $\mathbf{Q}(\mathbf{r})$. We employ here such a scaling that the scalar order parameter $S(\mathbf{r})$ is the eigenvalue of $\mathbf{Q}(\mathbf{r})$ corresponding to the nematic director $\mathbf{n}(\mathbf{r})$:

$$Q_{ij}(\mathbf{r}) = \frac{S(\mathbf{r})}{2}\left(3n_i(\mathbf{r})n_j(\mathbf{r}) - \delta_{ij}\right). \tag{27}$$

In the spirit of phenomenological Landau approach to the phase transitions of second order, a free energy functional of a liquid crystalline system is postulated in the form

$$F[\mathbf{Q}] = \int_V \left[f_{LdG}\Big(\mathbf{Q}(\mathbf{r})\Big) + f_{el}\Big(\nabla\mathbf{Q}(\mathbf{r})\Big) + f_H\Big(\mathbf{r}, \mathbf{Q}(\mathbf{r})\Big)\right] d^3r, \tag{28}$$

where $f_{LdG}(\mathbf{Q}(\mathbf{r}))$ (with $_{LdG}$ standing for Landau-de-Gennes) is a local and $f_{el}(\nabla\mathbf{Q}(\mathbf{r}))$ an elastic contributions, and $f_H(\mathbf{r}, \mathbf{Q}(\mathbf{r}))$ is a contribution due to the presence of an external magnetic (or electric) field. The equilibrium $\mathbf{Q}(\mathbf{r})$ minimizes $F[\mathbf{Q}]$, and the corresponding minimum of F equals to the free energy of the system.

- The Landau-de Gennes free energy density, and nematic-isotropic phase transition -

$f_{LdG}(\mathbf{Q}(\mathbf{r}))$ in Eq. (28) describes the nematic-isotropic phase transition in a spatially uniform system without external fields. According to the Landau phenomenological approach f_{LdG} is presented as a Taylor expansion in the scalar order parameter S. The series is truncated to the 4th power in S without losing the physics of the phase transition, but in general, there are higher order terms present. Because f_{LdG} is a scalar quantity, and $\mathbf{Q}$ is a second rank tensor with $Tr\mathbf{Q} = 0$, f_{LdG} must contain only scalar combinations of the order tensor: $Tr\mathbf{Q}^2 \sim S^2$ and $Tr\mathbf{Q}^3 \sim S^3$. The general form of f_{LdG} is then given by

$$f_{Ldg} = f_0 + a(T)Tr\mathbf{Q}^2 - bTr\mathbf{Q}^3 + c\left(Tr\mathbf{Q}^2\right)^2, \tag{29}$$

where f_0 is the free energy density of the isotropic phase. The presence of the term $\sim S^3$ reflects the fact that the nematic states described by S and $-S$ are distinct, and therefore the free energy is not symmetric with respect to the transformation $S \to -S$. In general, the coefficients a, b, and c in the Landau-de Gennes expansion (29) are temperature, T, dependent. To simplify the model, we assume that b and c are temperature independent positive constants. For spatially uniform systems Eq. (29) describes the coexistence between the nematic and isotropic phases. To this end we substitute (27) into expansion (29) and obtain

$$f_{LdG} = f_0 + \frac{3}{2}a(T)S^2 - \frac{3}{4}bS^3 + \frac{9}{4}cS^4, \tag{30}$$

which should be minimized with respect to S. It is convenient to define the dimensionless temperature $\tau = 24a(T)c/b^2$. The equation $\partial f_{LdG}/\partial S = 0$ has three solutions:

$$S_I = 0, (\text{the isotropic phase}) \tag{31}$$

$$S_N = \frac{b}{8c}\left(1 + \sqrt{1 - \frac{8\tau}{9}}\right) > 0, (\text{the nematic phase}). \tag{32}$$

The third solution

$$S_3 = \frac{b}{8c}\left(1 - \sqrt{1 - \frac{8\tau}{9}}\right) \tag{33}$$

should be disregarded as it corresponds either to a free energy maximum, with $S_3 > 0$, or to a metastable minimum ($f_{LdG}(S_3) > f_{LdG}(S_N)$) with $S_3 < 0$, see Fig. 5. The transition temperature T_{NI} and the corresponding value S_{NI} of the order parameter are defined from the condition that the free energy densities of the two phases are equal $f_{LdG}(S_{NI}) = f_0$ which gives

$$\begin{aligned} \tau_{NI} &= 1, \\ S_{NI} &= \frac{b}{6c}. \end{aligned} \tag{34}$$

The isotropic phase is unstable for $\tau < 0$, while the nematic becomes unstable for $\tau > 9/8$.

- Elastic free energy density -

The order tensor $\mathbf{Q}$ can depend on the spatial coordinates, which means that either the director $\mathbf{n}$ or the order parameter S (or all together) vary from place to place. This variation can be due to external forces imposed on the system, thermal fluctuations, or boundary conditions. Assuming these deformations

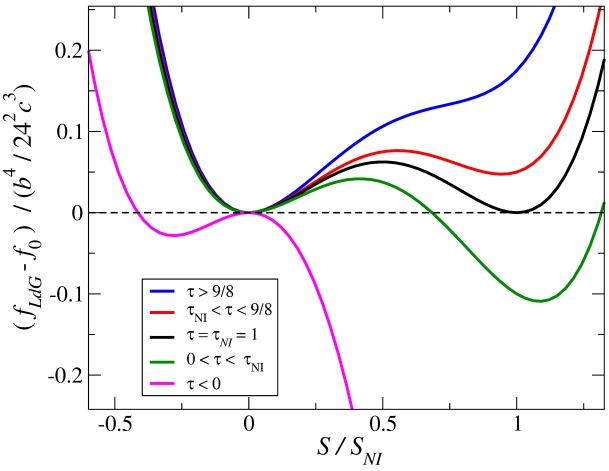

Figure 5: Landau-de Gennes free energy density (30) for uniaxial system as a function of scalar order parameter S for several values of reduced temperature $\tau = 24a(T)c/b^2$. At $\tau = \tau_{NI} = 1$ (black cure) the isotropic $S = 0$ and the nematic $S > 0$ phases coexist. For $1 < \tau < 9/8$ (red curve) the nematic phase is metastable, while for $\tau > 9/8$ (blue curve) the nematic phase is unstable. For $0 < \tau < 1$ (green curve) the isotropic phase is metastable, while for $\tau < 0$ the isotropic phase is unstable.

to vary slowly in space relative to the molecular distance scale, it is possible to describe the response of the liquid crystal using continuum elastic theory. Then the elastic free energy density can be written as

$$f_{el} = L_1 \frac{\partial Q_{ij}}{\partial x_k} \frac{\partial Q_{ij}}{\partial x_k} + L_2 \frac{\partial Q_{ij}}{\partial x_j} \frac{\partial Q_{ik}}{\partial x_k} + L_3 \frac{\partial Q_{ij}}{\partial x_k} \frac{\partial Q_{ik}}{\partial x_j}, \tag{35}$$

where L_1, L_2, and L_3 are the phenomenological constant parameters and the summation convention is assumed. In the case where the scalar order parameter S is constant, an expansion in terms of the director $\mathbf{n}$ is normally used to calculate elastic free energy density. Substituting Eq. (27) into (35) and using the condition $n_i n_i = 1$, f_{el} may be written in the form (modulo full divergences):

$$f_{el} = \frac{9S^2}{8}\Big((2L_1 + L_2 + L_3) (\nabla \cdot \mathbf{n})^2 + 2L_1 (\mathbf{n} \cdot [\nabla \times \mathbf{n}])^2 + (2L_1 + L_2 + L_3) [\mathbf{n} \times [\nabla \times \mathbf{n}]]^2 \Big) = \frac{1}{2}\Big(K_1 (\nabla \cdot \mathbf{n})^2 + K_2 (\mathbf{n} \cdot [\nabla \times \mathbf{n}])^2 + K_3 [\mathbf{n} \times [\nabla \times \mathbf{n}]]^2 \Big). \tag{36}$$

The second line represents the famous Frank-Oseen elastic free energy density for nematics with the splay K_1, twist K_2 and bend K_3 elastic constants:

$$K_1 = K_3 = \frac{9S^2}{4}(2L_1 + L_2 + L_3), K_2 = \frac{9S^2}{4}2L_1. \tag{37}$$

Examples of director configurations featuring these elastic modes are illustrated schematically in Fig. 6. For the purpose of qualitative calculations it is sometimes useful to assume that $K_1 = K_2 = K_3 = K$ (*one elastic constant approximation*). The elastic free energy density for this case reduces to

$$f_{el} = \frac{1}{2}K\left((\boldsymbol{\nabla}\cdot\mathbf{n})^2 + (\boldsymbol{\nabla}\times\mathbf{n})^2\right). \tag{38}$$

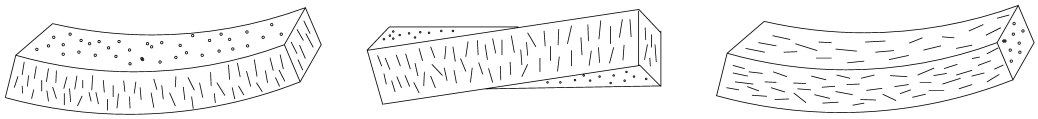

a b c

Figure 6: The three distinct elastic modes of a nematic liquid crystal: (a) splay with the contribution to the elastic free energy $K_1\left(\nabla\cdot\mathbf{n}\right)^2$, (b) twist: $K_2\left(\mathbf{n}\cdot[\nabla\times\mathbf{n}]\right)^2$, and (c) bend $K_3\left[\mathbf{n}\times[\nabla\times\mathbf{n}]\right]^2$. Typical values of $K_i \sim 10$pN.

- Response to external fields -

The director field is easily distorted and can be aligned by magnetic and electric fields, and by surfaces which have been properly prepared. We remind that the magnetic susceptibility tensor of a uniaxial liquid crystal has the form

$$\chi_{ij} = \chi_\perp\delta_{ij} + \chi_a n_i n_j, \tag{39}$$

where $\chi_a = \chi_\parallel - \chi_\perp$ is the anisotropy of the magnetic susceptibility, and is generally positive. It is thus possible to exert torques on the liquid crystal by applying a field. The presence of a magnetic field $\mathbf{H}$ contributes to the free energy density the following term

$$f_H = -\frac{\mu_0}{2}H_i\chi_{ij}H_j = -\frac{\mu_0}{2}\chi_\perp H^2 - \frac{\mu_0}{2}\chi_a(\mathbf{n}\cdot\mathbf{H})^2. \tag{40}$$

The first term in the rhs of Eq. (40) can be omitted as it is independent of the orientation of the director. The last term gives rise to a torque on the liquid crystal - if χ_a is positive the molecules will align parallel to the field.

The dielectric permittivity tensor of a liquid crystal is also anisotropic and has similar form as the magnetic susceptibility. Thus, in principle, we can achieve the same effect with an electric field as with a magnetic field. In an electric field **E** there will be an additional free energy contribution

$$f_E = -\frac{\varepsilon_0}{2}\varepsilon_\perp E^2 - \frac{\varepsilon_0}{2}\varepsilon_a(\mathbf{n}\cdot\mathbf{E})^2, \tag{41}$$

where $\varepsilon_\perp$ is the component of the relative dielectric permittivity tensor in the directions (degenerate) perpendicular to the director, $\varepsilon_a = \varepsilon_{||} - \varepsilon_\perp$ is the dielectric anisotropy, and ε_0 is the vacuum permittivity. In practice the alignment of a liquid crystal by an electric field is complicated by the presence of conducting impurities which make it necessary to use alternating electric fields.

5 Fréedericksz Transition

Consider a nematic liquid crystal between two glass slides. The interaction between the nematic and the glass is such that the director is constrained to lie *perpendicular* to the glass at the boundaries. When a magnetic field, applied perpendicular to the director, exceeds a certain critical value H_c, the optical properties of the system change abruptly. The reason is that both the magnetic field and the boundaries exert torques on the molecules and when the field exceeds H_c it becomes energetically favorable for the molecules in the bulk of the sample to turn in the direction of the field. This effect first observed by Fréedericksz and Zolina and can be used to measure some of the elastic constants.

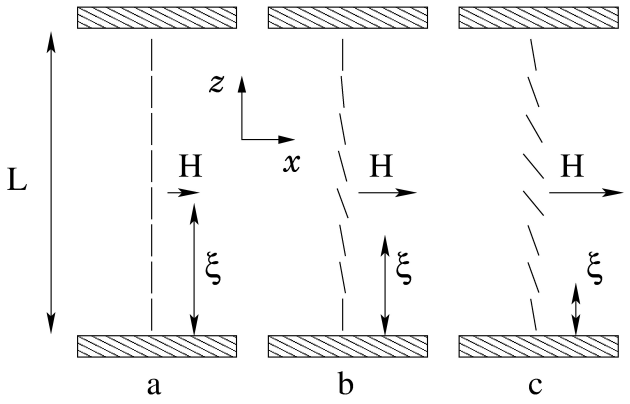

Figure 7: Fréedericksz transition. The liquid crystal is constrained to be perpendicular to the boundary surfaces and a magnetic field is applied in the x-direction. (a) Below a certain critical field H_c, the alignment is not affected. (b) Slightly above H_c, deviation of the alignment sets in. (c) Field is increased further, the deviation increases.

Let the z axis be perpendicular to the glass surfaces and the field **H** lie along the $x-$direction (see Fig. (7)). We parameterize the director as

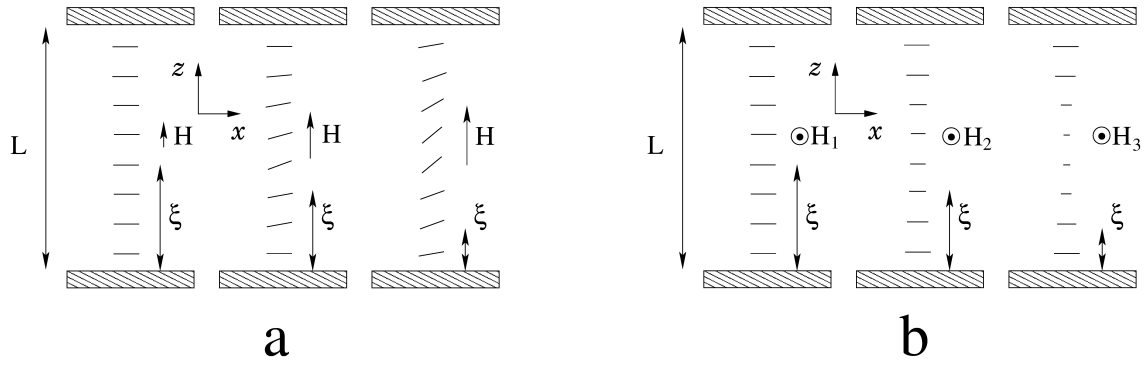

Figure 8: Schematic presentation of the setups for measuring K_1 in (a), and K_2 in (b) by using the magnetic Fréedericksz transition. (a) At the boundaries the liquid crystal is constrained to be parallel to the $x-$direction and a magnetic field is applied in the z-direction. (b) At the boundaries the liquid crystal is constrained to be parallel to the $x-$direction and a magnetic field is applied in the y-direction. $H_1 < H_2 < H_3$.

$$\mathbf{n} = \begin{pmatrix} \sin\theta(z) \\ 0 \\ \cos\theta(z) \end{pmatrix},$$

so that $\theta(z)$ is the angle between the director and the z axis. The elastic energy per unit area now takes the form

$$F_{el} = \frac{1}{2}\int_0^L dz \left(\left(K_1 \sin^2\theta + K_3 \cos^2\theta\right) \left(\frac{\partial\theta}{\partial z}\right)^2 - \mu_0 \chi_a H^2 \sin^2\theta \right), \tag{42}$$

L is the thickness of the sample. In the undistorted structure, $\theta = 0$, the field does not exert a torque on the molecules - they are in metastable equilibrium. Near the threshold H_c, distortions are weak, $\theta \ll 1$, and Eq. (42) writes in a simplified form

$$F_{el} \simeq \frac{K_3}{2}\int_0^L dz \left(\left(\frac{\partial\theta}{\partial z}\right)^2 - \frac{1}{\xi^2}\theta^2 \right), \tag{43}$$

where we define the length $\xi = \frac{1}{H_c}\sqrt{\frac{K_3}{\mu_0 \chi_a}}$. ξ can be interpreted as the distance which a disturbance can propagate into the liquid crystal in the presence of an ordering field. The length ξ is called the magnetic coherence length and arises in many problems involving the distortion produced by a magnetic field.

In order to estimate the threshold value of the field we use a variational *Ansatz*

$$\theta(z) = \theta_0 \sin\left(\frac{\pi z}{L}\right). \tag{44}$$

Substituting (44) into (43) and performing integration we obtain

$$F_{el} \simeq \frac{\pi^2 K_3}{4L}\left(1 - \left(\frac{L}{\pi\xi}\right)^2\right)\theta_0^2. \tag{45}$$

For $\xi > L/\pi$ the free energy in Eq. (45) is minimized at $\theta_0 = 0$, i.e., undistorted director configuration. We conclude that for weak fields

$$H < H_c \equiv \frac{\pi}{L}\sqrt{\frac{K_3}{\mu_0\chi_a}}, \tag{46}$$

the orienting strengths of the bounding surfaces "beats" the external field. For $\xi < L/\pi$, the prefactor in front of θ_0^2 in Eq. (45) is negative, signaling the instability of the undistorted $\theta = 0$ solution. This phenomena is named the Fréedericksz Transition. By measuring the threshold field H_c it is possible to calculate the bend elastic constant

$$K_3 = \mu_0\chi_a\left(\frac{H_c L}{\pi}\right)^2. \tag{47}$$

In the similar way it is possible to measure the splay K_1 and the twist K_2 elastic constants. The corresponding experimental setups are shown in Figs. (8)a, and b, respectively.

6 Optical Properties

It has already been mentioned above that the dielectric permittivity of a nematic is anisotropic and in a uniaxial state is a second-rank tensor

$$\epsilon_{ij} = \epsilon_\perp \delta_{ij} + \epsilon_a n_i n_j. \tag{48}$$

Correspondingly, we can introduce ordinary and extraordinary refractive indexes

$$n_e = \sqrt{\epsilon_\parallel}, \qquad n_o = \sqrt{\epsilon_\perp}, \qquad \Delta n = n_e - n_o. \tag{49}$$

For typical nematic liquid crystals, n_o is approximately 1.5 and the maximum difference, Δn, may range between 0.05 and 0.5.

Thus, when light enters a birefringent material, such as a nematic liquid crystal sample, the process is modeled in terms of the light being broken up into the fast (called the ordinary ray) and slow (called the extraordinary ray) components. The plane of polarization of the e-wave always contains the director

n, and the o-wave is always polarized normally to **n**. Because the two components travel at different velocities, the waves get out of phase. When the rays are recombined as they exit the birefringent material, the polarization state has changed because of this phase difference.

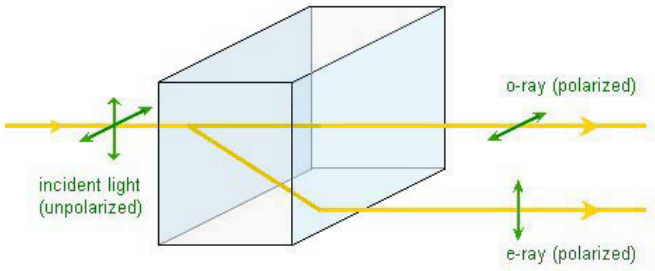

Figure 9: Light traveling through a birefringent medium will take one of two paths depending on its polarization.

The length of the sample is another important parameter because the phase shift accumulates as long as the light propagates in the birefringent material. Any polarization state can be produced with the right combination of the birefringence and length parameters.

Consider the case where a liquid crystal film is placed between crossed polarizers, see Fig. 10. The director $\mathbf{n}(x, y)$ is constrained to be in the (x, y) plane (the plane of the film). We assume that the incident light beam propagates along $z-$axis. A polarizer placed in front of the sample makes the incoming light linearly polarized along the polarizing direction $\boldsymbol{P}_{in} = (\cos\beta, \sin\beta)^T$. Upon entering into the nematic film this polarized wave splits into the ordinary component

$$\boldsymbol{E}_{\rm o}(z=0) = E_0 \begin{pmatrix} 0 \\ \sin\beta \end{pmatrix}, \tag{50}$$

and the extraordinary one

$$\boldsymbol{E}_{\rm e}(z=0) = E_0 \begin{pmatrix} \cos\beta \\ 0 \end{pmatrix}, \tag{51}$$

where $\beta(x, y)$ is the angle between $\mathbf{n}(x, y)$ and the polarization of the incoming wave, and $E_o = (\boldsymbol{E}_{in} \cdot \boldsymbol{P}_{in})$ is the projection of the incoming wave $\boldsymbol{E}_{in}$ onto $\boldsymbol{P}_{in}$. At the point of entry $z = 0$ into the nematic both waves are in phase. As was mentioned above, the two phase will need times $n_o d/c$ and $n_e d/c$ in order to pass through the film. At the exit point from the nematic film (but just before entering the analyzer) at $z = d$

$$\boldsymbol{E}_{\rm o}(z=d) = E_0 \sin\beta \mathrm{e}^{-i\omega t} \begin{pmatrix} 0 \\ \mathrm{e}^{ik_o d} \end{pmatrix}, \qquad \boldsymbol{E}_{\rm e}(z=d) = E_0 \cos\beta \mathrm{e}^{-i\omega t} \begin{pmatrix} \mathrm{e}^{ik_e d} \\ 0 \end{pmatrix}, \tag{52}$$

where $k_i = 2\pi n_i/\lambda_0$ are wave numbers of the ordinary $i = o$ and extraordinary $i = e$ waves, and λ_0 is the wave length in vacuum. Eq. (52) shows that at the exit point the two waves will gain a phase shift

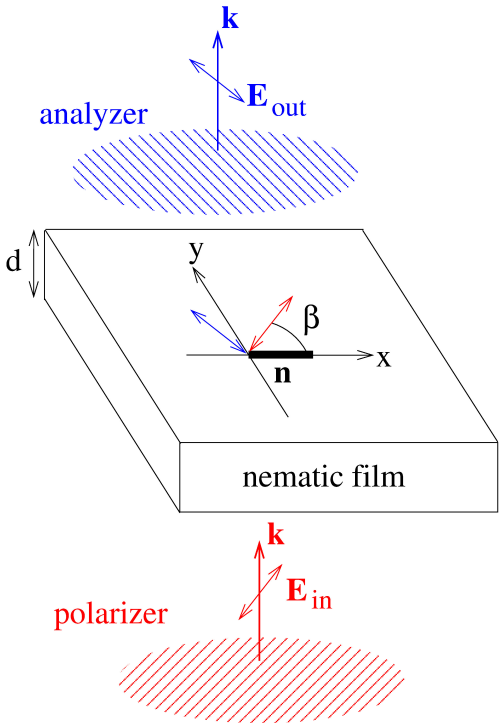

Figure 10: Schematic drawing of a light propagation trough a nematic film, placed between crossed polarizers. The polarization direction of the polarizer (depicted in red) in the local frame of reference shown on the nematic film can is given by $\boldsymbol{P}_{in} = (\cos\beta, \sin\beta)^T$, an the polarization direction of the analyzer (depicted in blue) is in the reference frame $\boldsymbol{P}_{out} = (-\sin\beta, \cos\beta)^T$.

$\delta\phi = (k_e - k_o)d$. Projecting the two waves onto the polarization direction $\boldsymbol{P}_{an} = (-\sin\beta, \cos\beta)^T$ of the analyzer and adding them we obtain the wave amplitude behind the analyzer

$$\boldsymbol{E}_{\rm out} = \Big(\Big[\boldsymbol{E}_{\rm o}(z=d) + \boldsymbol{E}_{\rm e}(z=d) \Big] \cdot \boldsymbol{P}_{out} \Big) \boldsymbol{P}_{out} = \frac{1}{2} E_0 \exp^{-i\omega t} \sin 2\beta (\mathrm{e}^{ik_o d} - \mathrm{e}^{ik_e d}) \begin{pmatrix} -\sin\beta \\ \cos\beta \end{pmatrix}. \quad (53)$$

The intensity of light $I = |\boldsymbol{E}_{\rm out}|^2$ passed through the system of crossed polarizers and the nematic films is

$$I = |E_0|^2 \sin^2 2\beta \sin^2 \left(\frac{\pi d}{\lambda_0} (n_e - n_o) \right). \quad (54)$$

Eq. (54) shows that for films of uniform thickness d the intensity pattern $I(x, y)$ of the transmitted light is determined by $\beta(x, y)$, i.e., by the in-plane configuration of the director field. In other words, the system of crossed polarizers maps the director field $\mathbf{n}(x, y)$ onto the transmitted light intensity $I(x, y)$.

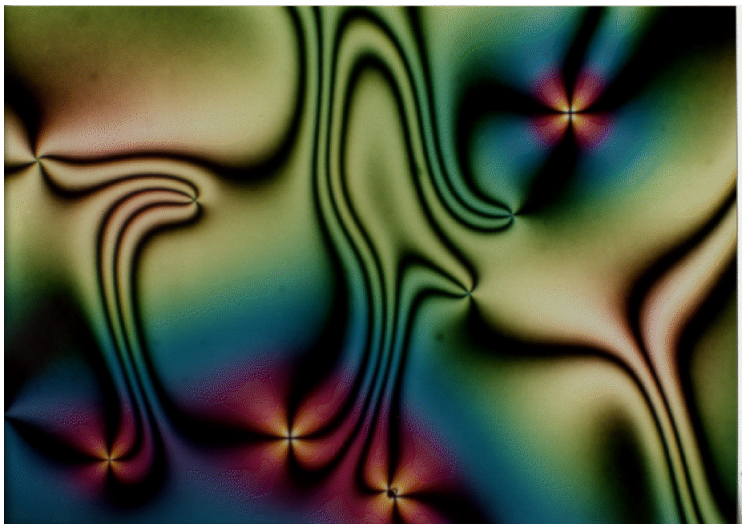

Figure 11: Schlieren texture of a nematic film with surface point defects. Dark brushes correspond to the regions where the director is parallel $\beta = 0$) or perpendicular ($\beta = \pm\pi/2$) to the polarizer. Points where four brushes meet correspond to the centers (cores) of topological point defects.

If the transmission axis of the first polarizer is parallel ($\beta = 0$) or perpendicular ($\beta = \pm\pi/2$) to the nematic director $\mathbf{n}$, the light is not broken up into components, and the corresponding region of the texture appears dark, see Fig. 11, where a texture with dark "brushes of extinction" is clearly visible. This type of textures is called the Schlieren texture. Points where four dark brushes meet are centers of topological defects. We note, that point topological defects can only exist in pairs. One can distinguish two types of defects with "opposite sign of the topological charge"; one type with yellow and red brushes, the other kind not that colorful. The difference in appearance is due to different core structures for these defects of different "charge". We note, that I also depends on the wavelength λ_0 and, therefore, for white light, the transmitted intensity will exhibit colorful textures, as shown in Fig. 11.

7 Topological Defects

Liquid crystals are ideal materials for studying topological defects. Distortions yielding defects are easily produced through control of boundary conditions, surface geometries, and external fields. The resulting defects are easily imaged optically. The simplest, *nematic* liquid crystalline phase owes its name to the typical *threadlike* defect which can be seen under a microscope in a nematic or cholesteric phase [2].

First explanations were given by Friedel [3] who suggested that these threads are lines on which the director changes its direction discontinuously. In analogy with dislocations in crystals, Frank proposed to call them *disclinations* [4]. To classify topological defects the homotopy theory can be employed to study the order parameter space [5]. For the case of nematics, there are two kinds of stable topological defects in three dimensions: point defects, called *hedgehogs* and line defects, called *disclinations*. Hedgehogs are characterized by an integer *topological charge* q specifying the number of times the unit sphere is wrapped by the director on any surface enclosing the defect core. An analytical expression for q is

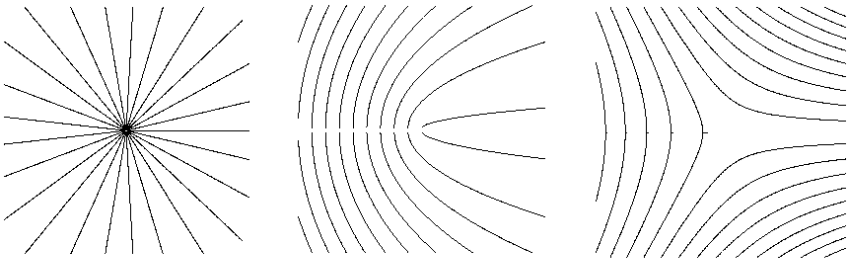

Figure 12: Examples of axial disclinations in a nematic: (a) $m = +1$, (b) the parabolic disclination, $m = +1/2$, (c) the hyperbolic disclination (topologically equivalent to the parabolic one), $m = -1/2$.

$$q = \frac{1}{8\pi} \int dS_i \epsilon_{ijk} \mathbf{n} \cdot (\partial_j \mathbf{n} \times \partial_k \mathbf{n}) \,, \tag{55}$$

where ∂_α denotes differentiation with respect to x_α, ϵ_{ijk} is the Levi-Civita symbol, and the integral is over any surface enclosing the defect core. For an order parameter with O_3, or vector symmetry, the order-parameter space is S^2, and hedgehogs can have positive or negative charges. Nematic inversion symmetry makes positive and negative charges equivalent, and we may, as a result, take all charges to be positive.

The axial director configurations representing disclination lines can be described in terms of the angle

$$\theta = m\phi + \theta_0, \tag{56}$$

where $n_x = \cos\theta, n_y = \sin\theta$, ϕ is the azimuthal angle, $x = r\cos\phi, y = r\sin\phi$, m is a positive or negative integer or half-integer [6]. Examples of disclinations for several m are given in Fig. (12). The elastic energy per unit length associated with a disclination is $\pi K m^2 \ln(R/r_0)$, where R is the size of the sample and r_0 is a lower cutoff radius (the core size) [6]. Since the elastic energy increases as m^2, the formation of disclinations with large Frank indices m is energetically unfavorable.

As has already been mentioned, within the continuum Frank theory, disclinations are singular lines where the gradient in the director becomes infinite; this signals a breakdown in the Frank theory. The region near the singularity where the Frank theory fails is called the disclination core. The phenomenological elastic theory predicts that a uniaxial nematic either melts or exhibits a complex biaxial structure in the core region [7].

Therefore, the core of the defect cannot be represented by the director field only, because of the possible biaxiality and variation of the order parameter. For this reason, a more general theory based on the alignment tensor should be applied to provide the correct description of the core region [8, 9, 10].

As we will discuss in the next section, topological defects appear naturally when a certain type of solid inclusions (colloidal particles) is introduced into liquid crystal.

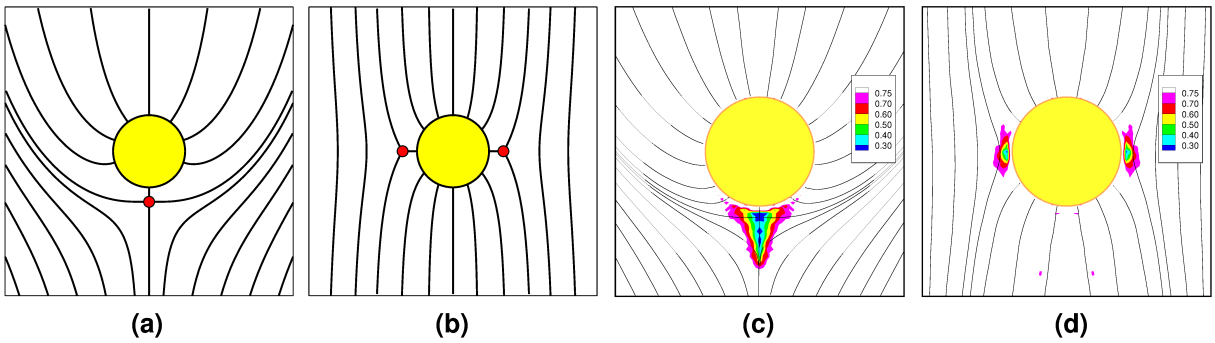

Figure 13: Sketches of (a) the satellite defect (dipole) and (b) the Saturn-ring defect (quadrupole) in the vicinity of a sphere with normal surface anchoring placed in a uniform aligned nematic. (c) and (d) show the corresponding scalar order parameter profiles and director maps obtained from the molecular dynamics simulations. Adapted from Ref. [11].

8 Colloidal Particles in Liquid Crystals

- An isolated colloidal particle -

In order to understand an effective interaction between particles dispersed in a nematic liquid crystal, it is essential to know the liquid crystal ordering near one of the particles. An isolated colloidal particle can provide either homeotropic (perpendicular to the surface) or tangential (parallel to it) boundary conditions for the nematic director. A particle with sufficiently strong homeotropic anchoring carries a topological charge of strength $+1$. If the director field is uniform far away from the particle, i. e. the total charge of the whole system is zero, an additional defect in the medium must be created in order to compensate the topological charge of the particle. Two defect types can arise in this case. The first one is a hyperbolic hedgehog, a point defect characterized by the topological charge of -1, called *satellite* defect. This particle-defect pair is usually modeled as a topological dipole because the asymptotic behavior of the director field has dipolar symmetry. The other possibility is a quadrupolar, or a *Saturn-ring* defect, that is a $-1/2$ strength disclination ring that encircles the particle. Both are sketched in Fig. 13.

Theoretical and numerical work based on the Frank-Oseen elastic free energy [12, 13, 14, 15] as well as experimental observations [16] suggest that the dipolar configuration is stable for the micron-sized particles usually considered experimentally. The Saturn-ring configuration should appear if the particle size is reduced and, when present, is always predicted to be most stable in the equatorial plane normal to the far field director.

- Effective pair interactions -

In a nematic solvent, elastic deformations of the director around particles lead to an additional, long-range, interaction. It can be of a dipolar or quadrupolar type, depending on the symmetry of the director configuration around particles.

The first experimental observations of these interactions were made in inverted nematic emulsions, that is water droplets dispersed in a nematic solvent [18]. The colloidal droplets formed linear chains, which were breaking upon transition to the isotropic phase. It was concluded that the liquid crystal host induces dipolar interaction which leads to droplet chaining, as well as a shorter range repulsive interaction [19].

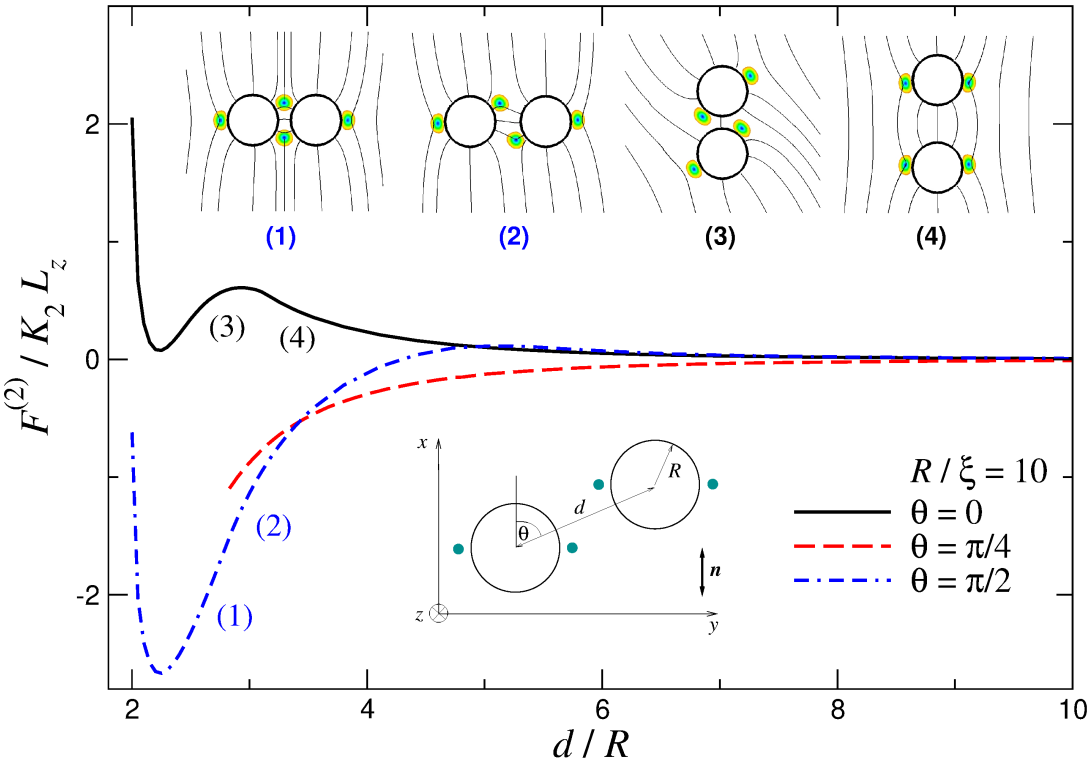

Figure 14: (Effective interaction potential (or potential of mean force) as a function of the separation d between two long cylindrical rods aligned along the z axis. Several angles θ between the far field director and the center-to-center vector are shown. The lower inset shows the z cross-section. The free energy is calculated by numerically minimizing the Landau-de Gennes free energy functional, Eqs. (29), (35). The far field director is along the x axis. The particle surfaces provide rigid homeotropic anchoring which gives rise to two disclination lines of topological charge of $-1/2$ at each particle. The alignment of the director and the variation of the scalar order parameter are shown in the top inset. The typical values for a nematic compound 5CB [17] are used in Eqs. (29), (35): $a = 0.06 \times 10^6\,\mathrm{J/m^3}$, $b = 0.816 \times 10^6\,\mathrm{J/m^3}$, $c = 0.45 \times 10^6\,\mathrm{J/m^3}$, $L_1 = 6 \times 10^{-12}\,\mathrm{J/m}$, $L_2 = 12 \times 10^{-12}\,\mathrm{J/m}$, and $L_3 = 0$. $K_2 = 9S_{\mathrm{bulk}}^2 L_1/2$. The nematic coherence length $\xi = \left(48 L_1 c/b^2\right)^{1/2} \approx 10\,\mathrm{nm}$, which corresponds to 5CB at a nematic-isotropic coexistence. The radius of colloidal particles is $R/\xi = 10$. The system size is $L_x \times L_y = 40R \times 40R$.

The large distance behavior of nematic-mediated interactions can be obtained from an electrostatic analogy by assuming that all constants in the expression for the elastic free energy, Eq. (36), are equal (one-constant approximation, $K_1 = K_2 = K_3 = K$) and by performing a multipole expansion of the director field [13, 20]. Indeed, far away from a colloidal particle, the director can be written in a linearized form, $\boldsymbol{n}(\boldsymbol{r}) = (n_x, n_y, 1 - O(n_x^2, n_y^2))$, and the Frank-Oseen elastic free energy, Eq. (36), reads as

$$F \simeq \frac{K}{2} \int d^3r \Big((\nabla n_x)^2 + (\nabla n_y)^2 + O(n_x^4, n_y^4) \Big). \tag{57}$$

Hence, the transverse director components, n_x and n_y, fulfill the Laplace equation. For a single particle, these can be expanded into multipoles. Using the superposition approximation, one can derive the following expressions for the effective pair potential

$$\begin{aligned} V_{\mathrm{dipole-dipole}} &\propto \frac{1 - 3\cos^2\theta}{d^3}, \\ V_{\mathrm{quadrupole-quadrupole}} &\propto \frac{9 - 90\cos^2\theta + 105\cos^4\theta}{d^5}, \\ V_{\mathrm{dipole-quadrupole}} &\propto \frac{\cos\theta}{d^4}(15\cos^2\theta - 9), \end{aligned} \tag{58}$$

where d is the distance between the particles and θ is the angle between the far field orientation of the nematic director (the z axis in our case) and the vector connecting the centers of the colloidal particles. These expressions can be generalized for particles of arbitrary shapes [21, 22, 23] or for weak anchoring at a particle surface [24].

The asymptotic behavior of the effective interaction potentials, given by Eqs. (58), has been directly measured for the dipole-dipole configuration corresponding to $\theta = 0$, using the free-release and the dual-beam optical tweezers methods. The quadrupolar tail of d^{-6} was also found experimentally for colloidal particles with the tangential boundary conditions [25, 26].

The electrostatic analogy of the linearized Frank-Oseen free energy in the one-elastic-constant approximation, Eq. (57), gives a good physical insight to understanding of structural properties of particle assemblies in dipolar [27], quadrupolar [28], or mixed [29, 30] situations. For example, the formation of long chains in the first, or rhomboidal structures in the last two cases can be inferred from the θ-angle dependence of the potentials in Eqs. (58).

However, at small separations, the situation becomes significantly more involved, since displacements of and interactions between topological defects lead to non-linear and many-body terms in the effective interaction potential. These short-range forces can be used to "synthesize colloidal molecules" [30] through a direct assembly using optical tweezers. Such aggregates are relatively stable objects made of dipolar and quadrupolar "colloidal atoms" which are bonded by topological defects. To obtain the free energy associated with a "chemical bond", one needs to refine the description of the nematic mesophase and to take into account the behavior of topological defects at small separations.

However, at small separations, the situation becomes significantly more involved, since displacements of and interactions between topological defects lead to non-linear and many-body terms in the effective interaction potential. These short-range forces can be used to "synthesize colloidal molecules" [30] through a direct assembly using optical tweezers. Such aggregates are relatively stable objects made of dipolar and quadrupolar "colloidal atoms" which are bonded by topological defects. To obtain the free energy associated with a "chemical bond", one needs to refine the description of the nematic mesophase and to take into account the behavior of topological defects at small separations.

Several approaches which go beyond the linearized theory and a simple superposition approximation have been proposed. Most popular are (i) numerical minimization of the Frank-Oseen elastic free energy functional in two and three spatial dimensions [14, 31, 32] (ii) minimization of the Landau-de Gennes free energy functional based on the five component tensorial order parameter [33, 34, 35, 36, 37, 38, 39, 40, 41], (iii) molecular dynamics [42] and Monte Carlo simulations [12], or using classical density functional theory [43, 44]. The results of these efforts can be summarized as follows. At small separations between

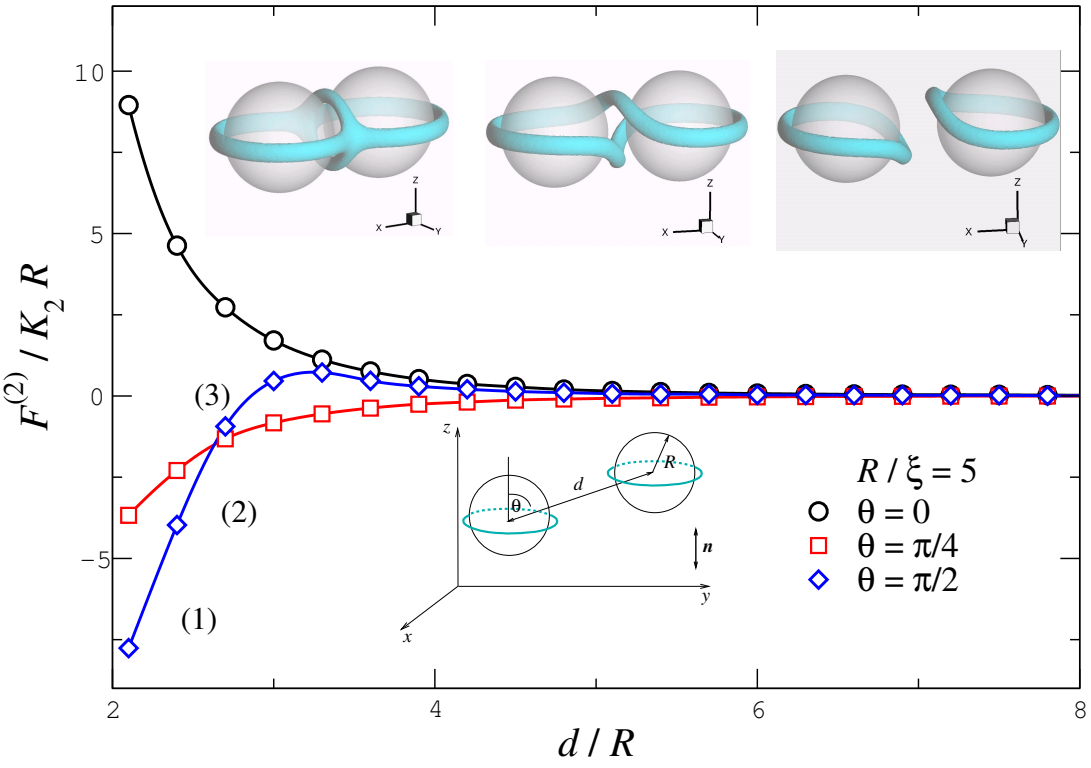

Figure 15: Effective interaction potential between two spherical colloidal particles as a function of separation d. The geometry is sketched in the lower inset. As before, the Landau de-Gennes free energy functional, Eqs. (29), (35), is minimized numerically using the finite elements method and adaptive meshes. Particles provide rigid homeotropic boundary conditions for the director. The surface scalar order parameter is fixed to the bulk value of the order parameter, $S_{\rm surface} = S_{\rm bulk}$. Material parameters used in Eqs. (29), (35) are similar to those used for cylindrical particles, see caption to Fig. 14, except that $a = 0.01 \times 10^6$ J/m^3. The upper inset depicts the nematic configurations for $\theta = \pi/2$ and several values of d. The blue rings around the particles show the iso-surfaces of the scalar order parameter corresponding to $S = S_{\rm bulk}/2$. The radius of colloidal particles is $R/\xi = 5$. The system size is $L_x \times L_y \times L_z = 30R \times 30R \times 30R$.

particles the topological defects rearrange their spatial position in order to minimize the free energy. This structural rearrangement changes the character of the effective interactions as compared to the asymptotic multipolar expressions in Eqs. (58). These changes are illustrated in Fig. 14 for the case of two long cylindrical and in Fig. 15 for two spherical colloidal particles. The mismatch in the boundary conditions at the surfaces of the particles and the bounding box produces compensating topological defects: accompanying disclination lines in the case of cylinders, and equatorial rings in the case of spheres. The spatial arrangement of these defects depends on the distance between the particles. In both cases, the far-field director distribution has quadrupolar symmetry, which results in d^{-4} and d^{-5} decay of the interaction potential for cylinders and spheres, respectively. However, at some separation, which depends on the angle θ and the particle type, repulsion between the particles changes to attraction. Switching between repulsion and attraction is more pronounced for cylinders than spheres, where it appears only for $\theta = \pi/2$. The insets of Figs. 14, 15 show that such behavior is due to the rearrangement of topological defects. For spherical particles, for example, two Saturn rings (equatorial defects) merge into one at small separations.

References

[1] L. Onsager. The effects of shape on the interaction of colloidal particles. *Ann. N. Y. Acad. Sci.*, 51:627, 1949.

[2] D. Demus and L. Richter. *Textures of Liquid Crystals.* Verlag Chemie, Weinheim, 1978.

[3] G. Friedel. *Ann. Phys. (Paris)*, 19:273, 1922.

[4] F. C. Frank. *Discuss. Faraday Soc.*, 25:19, 1978.

[5] N. D. Mermin. Topological theory of defects in ordered media. *Rev. Mod. Phys.*, 51:591–648, 1979.

[6] M.J. Stephen and J.P Straley. Physics of liquid crystals. *Rev. Mod. Phys.*, 46:617–704, 1974.

[7] P. Biscari. Intrinsically biaxial systems: A variational theory for elastomers. *Mol. Cryst. Liq. Cryst. Sci. Technol. Sect. A-Mol. Cryst. Liq. Cryst.*, 299:235–243, 1997.

[8] N. Schopohl and T. J. Sluckin. Defect core structure in nematic liquid crystals. *Phys. Rev. Lett.*, 59:2582–2584, 1987.

[9] N. Schopohl. Correction. *Phys. Rev. Lett.*, 60:755–755, 1988.

[10] A. Sonnet, A. Kilian, and S. Hess. Alignment tensor versus director - description of defects in nematic liquid-crystals. *Phys. Rev. E*, 52:718–722, 1995.

[11] Denis Andrienko, Guido Germano, and Michael P. Allen. Computer simulation of topological defects around a colloidal particle or droplet dispersed in a nematic host. *Phys. Rev. E*, 63:041701, 2001.

[12] R. W. Ruhwandl and E. M. Terentjev. Monte carlo simulation of topological defects in the nematic liquid crystal matrix around a spherical colloid particle. *Phys. Rev. E*, 56:5561–5565, 1997.

[13] T. C. Lubensky, David Pettey, Nathan Currier, and Holger Stark. Topological defects and interactions in nematic emulsions. *Phys. Rev. E*, 57(1):610–625, Jan 1998.

[14] H. Stark. Director field configurations around a spherical particle in a nematic liquid crystal. *Euro. Phys. J. B*, 10:311–321, 1999.

[15] S. Grollau, N. L. Abbott, and J. J. de Pablo. Spherical particle immersed in a nematic liquid crystal: Effects of confinement on the director field configurations. *Phys. Rev. E*, 67(1):011702, Jan 2003.

[16] Yuedong Gu and Nicholas L. Abbott. Observation of saturn-ring defects around solid microspheres in nematic liquid crystals. *Phys. Rev. Lett.*, 85(22):4719–4722, Nov 2000.

[17] S Kralj, S Zumer, and D. W. Allender. Nematic-isotropic phase-transition in a liquid-crystal droplet. *Phys. Rev. A*, 43(6):2943–2954, MAR 1991.

[18] P Poulin, H Stark, T. C. Lubensky, and D. A. Weitz. Novel colloidal interactions in anisotropic fluids. *Science*, 275(5307):1770–1773, MAR 1997.

[19] H Stark. Physics of colloidal dispersions in nematic liquid crystals. *Phys. Rep.*, 351(6):387–474, OCT 2001.

[20] S Ramaswamy, R Nityananda, V A Raghunathan, and J Prost. Power-law forces between particles in a nematic. *Mol. Cryst. Liq. Cryst.*, 288:175–180, 1996.

[21] B. I. Lev and P. M. Tomchuk. Interaction of foreign macrodroplets in a nematic liquid crystal and induced supermolecular structures. *Phys. Rev . E*, 59(1):591–602, Part A JAN 1999.

[22] B. I. Lev, S. B. Chernyshuk, P. M. Tomchuk, and H Yokoyama. Symmetry breaking and interaction of colloidal particles in nematic liquid crystals. *Phys. Rev . E*, 65(2):–, Part 1 FEB 2002.

[23] B. I. Lev, H Yokoyama, S. B. Chernyshuk, and P. M. Tomchuk. Symmetry breaking, elastic interaction and structures in nematic colloids. *Mol. Cryst. Liq. Cryst.*, 409:99–109, 2004.

[24] R. W Ruhwandl and E. M. Terentjev. Long-range forces and aggregation of colloidal particles in a nematic liquid crystal. *Phys. Rev. E*, 55:2958–2961, 1997.

[25] J Kotar, M Vilfan, N Osterman, D Babic, M Copic, and I Poberaj. Interparticle potential and drag coefficient in nematic colloids. *Phys. Rev. Lett.*, 96(20):207801, MAY 2006.

[26] I. I. Smalyukh, O. D. Lavrentovich, A. N. Kuzmin, A. V. Kachynski, and P. N. Prasad. Elasticity-mediated self-organization and colloidal interactions of solid spheres with tangential anchoring in a nematic liquid crystal. *Phys. Rev. Lett.*, 95(15):157801, OCT 7 2005.

[27] M Skarabot, M Ravnik, S Zumer, U Tkalec, I Poberaj, D Babic, N Osterman, and I Musevic. Two-dimensional dipolar nematic colloidal crystals. *Phys. Rev. E*, 76(5):051406, Part 1 NOV 2007.

[28] M Skarabot, M Ravnik, S Zumer, U Tkalec, I Poberaj, D Babic, N Osterman, and I Musevic. Interactions of quadrupolar nematic colloids. *Phys. Rev. E*, 77(3):031705, Part 1 MAR 2008.

[29] U Ognysta, A Nych, V Nazarenko, I Musevic, M Skarabot, M Ravnik, S Zumer, I Poberaj, and D Babic. 2d interactions and binary crystals of dipolar and quadrupolar nematic colloids. *Phys. Rev. Lett.*, 100(21):217803, MAY 2008.

[30] U Ognysta, A Nych, V Nazarenko, M Skarabot, and I Musevic. Design of 2d binary colloidal crystals in a nematic liquid crystal. *Langmuir*, 25(20):12092–12100, Feb. 2009.

[31] P Patrício, M Tasinkevych, and M. M. T da Gama. Colloidal dipolar interactions in 2d smectic-c films. *Eur. Phys. J. E*, 7(2):117–122, June 2002.

[32] K. S. Korolev and D. R. Nelson. Defect-mediated emulsification in two dimensions. *Phys. Rev. E*, 77(5):051702, Part 1 MAY 2008.

[33] C Zhou, P Yue, and JJ Feng. Dynamic simulation of droplet interaction and self-assembly in a nematic liquid crystal. *Langmuir*, 24(7):3099–3110, APR 1 2008.

[34] Jun-ichi Fukuda, H Stark, M Yoneya, and H Yokoyama. Interaction between two spherical particles in a nematic liquid crystal. *Phys. Rev. E*, 69(4):041706, Part 1 APR 2004.

[35] Jun-ichi Fukuda, H Yokoyama, M Yoneya, and H Stark. Interaction between particles in a nematic liquid crystal: Numerical study using the landau-de gennes continuum theory. *Mol. Cryst. Liq. Cryst.*, 435:723–734, 2005.

[36] M Tasinkevych, NM Silvestre, P Patricio, and MMT da Gama. Colloidal interactions in two-dimensional nematics. *Eur. Phys. J. E*, 9(4):341–347, NOV 2002.

[37] O Guzman, E. B. Kim, S Grollau, N. L. Abbott, and J. J. de Pablo. Defect structure around two colloids in a liquid crystal. *Phys. Rev. Lett.*, 91(23):235507, DEC 5 2003.

[38] N. M Silvestre, P Patrício, M Tasinkevych, Denis Andrienko, and M. M. T da Gama. Colloidal discs in nematic liquid crystals. *J. Phys.: Condens. Matter*, 16(19):S1921–S1930, Sp. Iss. SI MAY 2004.

[39] Jun-ichi Fukuda and H Yokoyama. Separation-independent attractive force between like particles mediated by nematic-liquid-crystal distortions. *Phys. Rev. Lett*, 94(14):148301, APR 2005.

[40] F. R. Hung. Quadrupolar particles in a nematic liquid crystal: Effects of particle size and shape. *Phys. Rev. E*, 79(2):021705, Part 1 FEB 2009.

[41] M Ravnik and S Zumer. Landau-de gennes modelling of nematic liquid crystal colloids. *Liquid Crystals*, 36:1201–1214, 2009.

[42] D Andrienko, M Tasinkevych, P Patrício, M P Allen, and M. M. T da Gama. Forces between elongated particles in a nematic colloid. *Phys. Rev. E*, 68(5):051702, Part 1 NOV 2003.

[43] D. L. Cheung and M. P. Allen. Liquid-crystal-mediated force between a cylindrical nanoparticle and substrate. *Phys. Rev. E*, 76(4):041706, Part 1 OCT 2007.

[44] D. L. Cheung and M. P. Allen. Forces between cylindrical nanoparticles in a liquid crystal. *Langmuir*, 24(4):1411–1417, FEB 2008.